Chinese Physics Letters

LETTER

Spin-Excitation Response to Oxygen Deficiency in $La_3Ni_2O_{7-\delta}$ Thin Films

Cite as: Hengyang Zhong *et al*. 2026 *Chin. Phys. Lett.* **43** 060717

DOI CSTR

Recommended Articles

Superexchanges and Charge Transfer in $La_3Ni_2O_7$ Thin Films

Yuxun Zhong, Wéi Wú, and Dao-Xin Yao
Chin. Phys. Lett. **43**, 030713 (2026)

Microscopic Evidence of Charge- and Spin-Density Waves in $La_3Ni_2O_{7-\delta}$ Revealed by ^{139}La-NQR

Jun Luo, Jie Feng, Gang Wang, Ningning Wang, Jie Dou, Aifang Fang, Jie Yang, Jinguang Cheng, Guoqing Zheng, and Rui Zhou
Chin. Phys. Lett. **42**, 067402 (2025)

The Effect of Carrier Doping and Thickness on the Electronic Structures of $La_3Ni_2O_7$ Thin Films

Haoliang Shi, Zihao Huo, Guanlin Li, Hao Ma, Tian Cui, Daoxin Yao, and Defang Duan
Chin. Phys. Lett. **42**, 080708 (2025)

Tuning of the Metal–Insulator Transition in Nd-Doped Bilayer Nickelate $La_3Ni_2O_7$ Thin Films

Fang-Hui Zhu, Xue-Yan Wang, Ting-Na Shao, Qiang Zhao, Wen-Long Yang, Cheng-Xue Chen, Mei-Ling Yan, Rui-Fen Dou, Chang-Min Xiong, and Jia-Cai Nie
Chin. Phys. Lett. **42**, 067303 (2025)

Normal and Superconducting Properties of $La_3Ni_2O_7$

Meng Wang, Hai-Hu Wen, Tao Wu, Dao-Xin Yao, and Tao Xiang
Chin. Phys. Lett. **41**, (2024)

High-Temperature Superconductivity in $La_3Ni_2O_7$

Kun Jiang, Ziqiang Wang, and Fu-Chun Zhang
Chin. Phys. Lett. **41**, (2024)

A series journal of Chinese Physical Society distributed by IOP Publishing

Chinese Physics Letters

Chin. Phys. Lett. **43** 060717 (2026)

LETTER

DOI: 10.1088/0256-307X/43/6/060717
CSTR: 32039.14.0256-307X.43.6.060717

Spin-Excitation Response to Oxygen Deficiency in $La_3Ni_2O_{7-\delta}$ Thin Films

Hengyang Zhong[1,†,*], Bo Hao[2,3,†], Anni Chen[4], Xinru Huang[1], Chunyi Li[1], Wenting Zhang[1], Chang Liu[1], Kurt Kummer[5], Nicholas Brookes[5], Yuefeng Nie[2,3,*], Thorsten Schmitt[4,*], and Xingye Lu[1,*]

[1]Center for Advanced Quantum Studies, School of Physics and Astronomy, and Key Laboratory of Multiscale Spin Physics (Ministry of Education), Beijing Normal University, Beijing 100875, China
[2]National Laboratory of Solid State Microstructures, Jiangsu Key Laboratory of Artificial Functional Materials, College of Engineering and Applied Sciences, Nanjing University, Nanjing 210093, China
[3]Collaborative Innovation Center of Advanced Microstructures, Nanjing University, Nanjing 210093, China
[4]Photon Science Division, Swiss Light Source, Paul Scherrer Institut, CH-5232 Villigen PSI, Switzerland
[5]European Synchrotron Radiation Facility, BP 220, F-38043 Grenoble Cedex, France

[†]These authors contributed equally to this work.
[*]Corresponding authors. Email: hengyang_zhong@mail.bnu.edu.cn; ynie@nju.edu.cn; thorsten.schmitt@psi.ch; luxy@bnu.edu.cn

Oxygen stoichiometry has been identified as a key parameter controlling superconductivity in the bilayer nickelate $La_3Ni_2O_{7-\delta}$. Using resonant inelastic x-ray scattering, we systematically investigate the evolution of orbital and spin excitations in $La_3Ni_2O_{7-\delta}$ thin films with varying oxygen content. In vacuum-annealed samples, the suppression of the 1.6 eV dd excitation under π polarization reflects appreciable inner apical-oxygen vacancies, which locally disrupt the out-of-plane p–d hybridization and the corresponding interlayer superexchange pathways. Nevertheless, the oxygen-deficient films exhibit spin excitations originating from Q = (0.25, 0.25) with a similar dispersion to the as-grown sample, suggesting a mixed ground state of double spin stripe and spin-charge stripe orders with nearly identical spin correlations. By contrast, the magnon damping rate is slightly enhanced in the vacuum-annealed sample, reflecting a modest increase in electronic disorder associated with oxygen defects. Collectively, these findings reveal that short-range spin correlations in $La_3Ni_2O_{7-\delta}$ are insensitive to oxygen-vacancy-induced perturbations, including electron doping and local disruption of interlayer superexchange pathways, even in samples with appreciable oxygen deficiency, where the 1.6 eV dd excitation associated with Ni $3d_{z^2}$-O $2p_z$ hybridization is suppressed by up to 58%.

The discovery of superconductivity with an onset superconducting temperature ($T_{c,onset}$) of around 80 K under high pressure of ~14 GPa in $La_3Ni_2O_{7-\delta}$ [1] has stimulated tremendous experimental and theoretical research on this new high-T_c superconductor family. A key characteristic of this material is the high sensitivity of its transport properties to oxygen stoichiometry [1–8], which confines superconductivity to a narrow window of oxygen content [1,6–11]. More recently, ambient-pressure superconductivity has been realized in epitaxially strained thin films, with $T_{c,onset}$ initially limited to ~40 K [12–14]. Subsequent improvements have pushed $T_{c,onset}$ to above 48 K [15] and through precise optimization of oxygen stoichiometry further to ~60 K [16]. These advances highlight the central role of oxygen stoichiometry in stabilizing superconductivity and reshaping the low-energy physics in this bilayer nickelate.

$La_3Ni_2O_{7-\delta}$ is a bilayer Ruddlesden–Popper (RP) nickelate, in which two NiO_2 layers form the superconducting planes. The oxygen sites can be classified into three types: in-plane oxygen, inner apical oxygen (O_{AP}), and outer apical oxygen [Fig. 1(a)]. Among these, oxygen vacancies in bulk $La_3Ni_2O_{7-\delta}$ primarily occur at the O_{AP} sites [17], whereas in $La_3Ni_2O_{7-\delta}$ films grown on $SrLaAlO_4$ (SLAO) substrates under a large compressive strain of approximately −2%, the vacancies are predominantly found at the in-plane oxygen sites [14]. The NiO_6 octahedral crystal field splits the Ni 3d orbitals into e_g and t_{2g} manifolds, with the e_g states dominating the low-energy physics [1,18–26]. Among them, the nearly half-filled Ni d_{z^2} orbital is relatively localized and strongly correlated, whereas the nearly quarter-filled Ni $d_{x^2-y^2}$ orbital is more itinerant and weakly correlated [19,23–25]. The two NiO_2 layers within a unit cell are strongly coupled via Ni d_{z^2}-O_{AP} p_z hybridization, resulting in a large interlayer antiferromagnetic superexchange interaction J_z [1,27], which distinguishes $La_3Ni_2O_{7-\delta}$ from cuprate superconductors [28–33]. Importantly, RIXS measurements have established that this interlayer superexchange J_z is much larger than the intralayer exchange interactions [34], and further revealed that its evolution under epitaxial strain closely tracks the emergence of superconductivity [35], supporting a superconducting pairing scenario driven by J_z, assisted by Hund's coupling [25,36–43] or by inter-orbital hybridization between the Ni d_{z^2} and $d_{x^2-y^2}$ orbitals [44–53].

Oxygen vacancies generally exist in $La_3Ni_2O_{7-\delta}$ and would effectively introduce electron carriers [54]. Theoretically, the electronic and magnetic properties are expected to be highly sensitive to oxygen vacancies. Specifically, O_{AP} vacancies disrupt the local Ni-O_{AP}-Ni interlayer hopping channel, thereby diluting the interlayer superexchange interaction [42,55]. At the same time, they increase the local on-site energy near the vacancy, leading to a decreased electronic density of states (DOS) [42]. Moreover, oxygen vacancies tend to generate local magnetic moments at the vacant sites [56–58], whose random distribution can degrade electronic coherence and further drive Anderson localization [57,58]. In addition, oxygen vacancies convert nearby Ni sites into spinless charge sites, driving the ground state toward a mixed order of double spin stripe (DSS) and spin-charge stripe (SCS) [55].

However, a direct experimental determination of how oxygen deficiencies modify the spin dynamics remains lacking. In particular, it remains unclear whether the dominant interlayer superexchange energy scale survives substantial oxygen vacancies, or whether oxygen deficiency primarily affects other aspects of the electronic structure, such as orbital hybridization and electronic coherence. In this context,

Received 16 March 2026; accepted 7 May 2026; published 17 June 2026
© 2026 Chinese Physical Society and IOP Publishing Ltd. All rights, including for text and data mining, AI training, and similar technologies, are reserved.

Check for updates

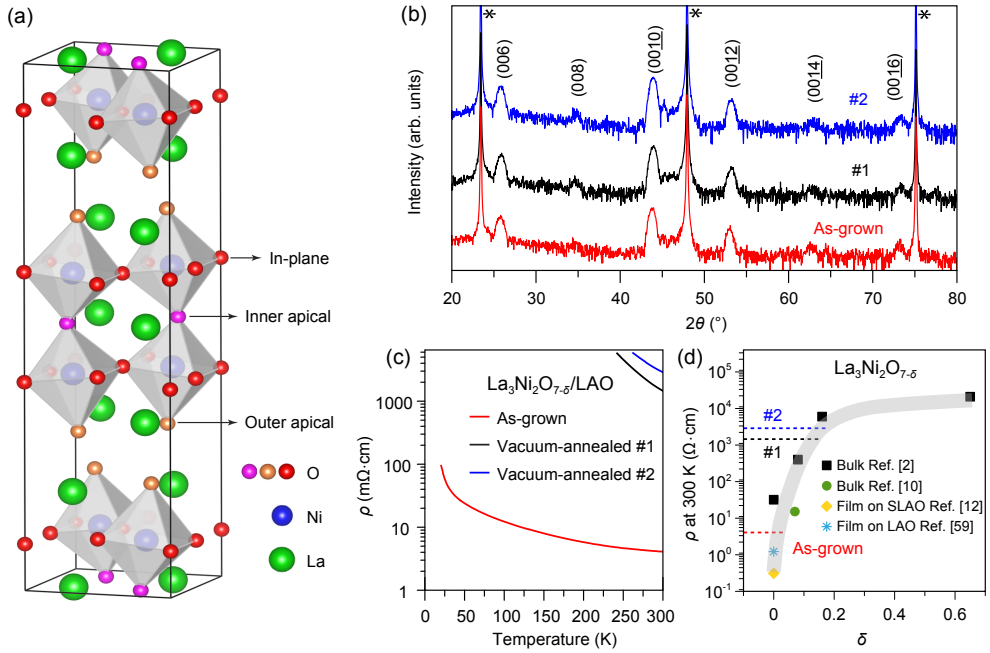

Fig. 1. (a) Crystal structure of orthorhombic Amam $La_3Ni_2O_{7-\delta}$ with three types of oxygen atoms, indicated as red, pink, and orange spheres. (b) X-ray diffraction (XRD) θ-2θ scans of as-grown and vacuum-annealed $La_3Ni_2O_{7-\delta}$/LAO thin films. The $La_3Ni_2O_{7-\delta}$ $(00L)$ diffraction peaks were labeled. The LAO diffraction peaks are indicated as black stars. (c) Temperature dependence of resistivity (ρ) of as-grown and vacuum-annealed $La_3Ni_2O_{7-\delta}$/LAO thin films. Sample #1 (black curve) and sample #2 (blue curve) were vacuum-annealed at 300 ℃ for 30 minutes, and at 400 ℃ for 60 minutes, respectively. The resistivity data for as-grown $La_3Ni_2O_{7-\delta}$/LAO are taken from Ref. [35]. (d) Summary of ρ at 300 K for bulk $La_3Ni_2O_{7-\delta}$ [2,10], superconducting $La_3Ni_2O_{7-\delta}$/LAO [59] as well as $La_3Ni_2O_{7-\delta}$/SLAO [12], and $La_3Ni_2O_{7-\delta}$/LAO in this work. The gray line is a guide to the eye.

resonant inelastic x-ray scattering (RIXS) provides a uniquely powerful probe, as it enables direct measurements of momentum-resolved spin excitations as well as element-selective orbital excitations [60]. By systematically tracking the evolution of magnetic and orbital excitations with oxygen stoichiometry, RIXS provides direct insight into how oxygen vacancies modify the low-energy spin and orbital degrees of freedom.

In this work, we use Ni-L_3 RIXS to investigate the response of spin and electronic excitations to oxygen deficiencies in as-grown and vacuum-annealed $La_3Ni_2O_{7-\delta}$ thin films grown on $LaAlO_3$ (LAO) substrates. Incident-energy-dependent RIXS measurements reveal a strong suppression of localized dd excitations in the vacuum-annealed films, most notably the $\sim$1.6 eV dd excitation associated with Ni $3d_{z^2}$-O_{AP} p_z hybridized states [35,61]. This provides direct evidence for an appreciable concentration of O_{AP} vacancies, which locally disrupt the interlayer Ni-O_{AP}-Ni superexchange pathway that mediates J_z. Strikingly, high-resolution RIXS reveals that, despite this local disruption, the collective spin excitations remain largely unchanged in their dispersion, spectral weight, and overall energy scale. Moreover, the dispersion originates from $Q = (0.25, 0.25)$. This is consistent with a mixed DSS and SCS magnetic ground state theoretically predicted for $La_3Ni_2O_{7-\delta}$ $(0 < \delta < 0.5)$ [55], as both magnetic orders possess an identical propagation vector $Q_{SDW} = (0.25, 0.25)$ and nearly indistinguishable spin correlations [34]. The spin-excitation dispersion remains robust against oxygen deficiency in our vacuum-annealed films, demonstrating that short-range spin correlations are insensitive to both the local disruption of J_z and the electron doping induced by appreciable oxygen vacancies. Instead, randomly distributed oxygen vacancies slightly introduce disorder and reduce electronic coherence, as reflected in the modest broadening of the magnon linewidth. These results elucidate the complex interplay between magnetism and oxygen deficiencies in bilayer nickelates, providing important insight into the superconducting mechanism.

$La_3Ni_2O_{7-\delta}$ thin films were epitaxially grown on atomically flat and AlO_2-terminated LAO (001) substrate surfaces by reactive molecular-beam epitaxy (MBE) in a DCA R450 system at substrate temperatures of around 600 ℃ and under an oxidant atmosphere at 1×10^{-5} Torr, with the thickness precisely controlled to five unit cells. The oxygen deficiency was artificially introduced by post-growth vacuum annealing at a base pressure of $\sim 1 \times 10^{-3}$ Torr at 300 ℃ for 30 minutes for sample #1, and at 400 ℃ for 60 minutes for sample #2. High crystalline quality of the films was confirmed by X-ray diffraction (XRD) θ-2θ scans using a monochromatized Cu $K_{\alpha 1}$ source ($\lambda = 1.5406$ Å) [Fig. 1(b)], which show that all samples crystallize in the bilayer RP phase with no detectable additional RP phases. RIXS measurements were performed at the ID32 beamline of the European Synchrotron Radiation Facility (ESRF). All data were collected at 20 K with π-polarized incident X-rays. Incident-energy-dependent RIXS spectra were measured near the Ni-L_3 edge at a grazing incident angle of $\theta = 20°$. Momentum-dependent RIXS spectra were measured at an incident energy $E_i = 856.4$ eV in a $2\theta = 90°$ scattering geometry, along the two high-symmetry directions $[H, 0]$ and $[H, H]$, with an energy resolution of $\Delta E \approx 32$ meV. Pseudo-tetragonal primitive vectors with $a_T = b_T = 3.792$ Å were adopted in this work.

Figure 1(c) displays the temperature-dependent resistivity of the $La_3Ni_2O_{7-\delta}$/LAO thin films. The vacuum-annealed samples #1 and #2 become significantly insulating due to the formation of oxygen vacancies. Figure 1(d) summarizes the resistivity at 300 K for several $La_3Ni_2O_{7-\delta}$ samples with different δ values [2,10,12,59], together with the $La_3Ni_2O_{7-\delta}$/LAO films investigated in this work. Since the $La_3Ni_2O_{7-\delta}$/LAO film with compressive strain $(\varepsilon) \sim -1\%$ in Ref. [59] and the $La_3Ni_2O_{7-\delta}$/$SrLaAlO_4$ film with $\varepsilon \sim -2\%$ in Ref. [12] exhibit superconductivity, they can be considered nearly stoichiometric ($\delta \approx 0$). The resistivity of $La_3Ni_2O_{7-\delta}$ is known to be influenced by multiple factors, including oxygen content, epitaxial strain, stacking defects, and phase purity. Nevertheless, the impact of strain [62], stacking defects [12], and phase purity [63,64] on the magnitude of the resistivity is considerably weaker than that of the oxygen content [2]. Therefore, figure 1 provides a rough estimate of the oxygen vacancy concentration range for our samples. However, it must be emphasized that this empirical approach cannot yield a precise quantitative determination of δ.

Figure 2(a) displays an incident-energy-dependent RIXS map of an as-grown $La_3Ni_2O_{7-\delta}$/LAO thin film near the Ni-L_3 edge, overlaid

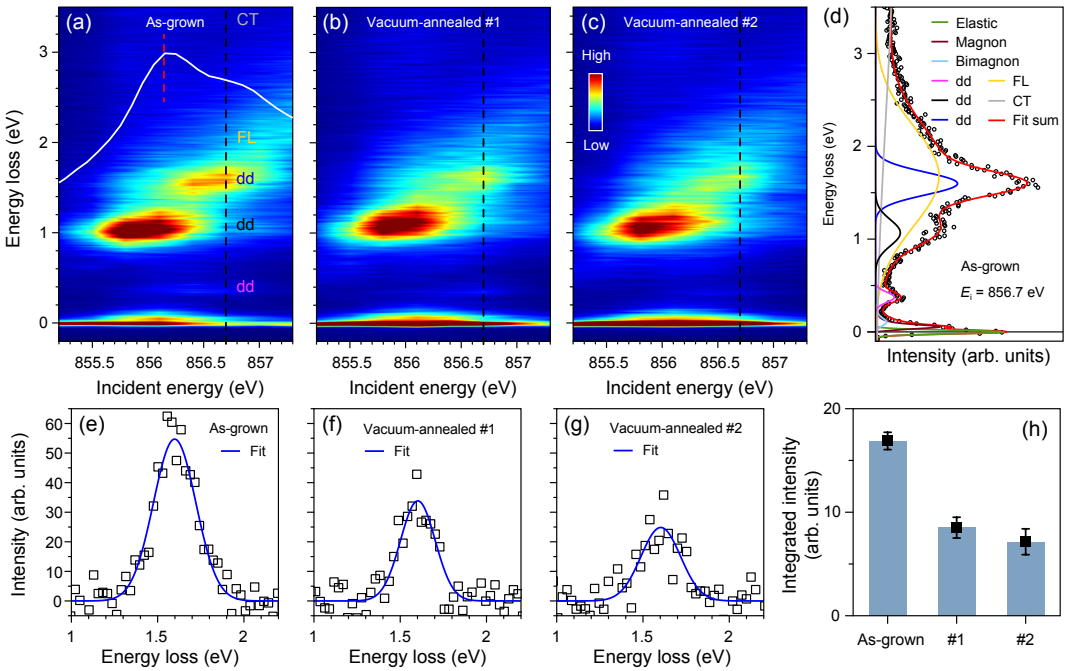

Fig. 2. (a)–(c) Incident-energy-dependent RIXS maps of as-grown and vacuum-annealed $La_3Ni_2O_{7-\delta}$/LAO thin films. Measurements were performed at 20 K with π polarization at $2\theta_s = 150°$ and $\theta = 20°$. All RIXS spectra were normalized to the incident photon flux. The white curve in panel (a) displays the total fluorescence yield (TFY) XAS of the as-grown film after subtracting the La-M_4 peak, measured under the same experimental geometry. (d) Fitting plot of the RIXS spectrum at $E_i = 856.7$ eV for as-grown $La_3Ni_2O_{7-\delta}$/LAO. The high-energy inelastic response, three types of dd excitations, fluorescence (FL) and charge-transfer excitations (CT), are marked at the corresponding positions in panel (a). (e)–(g) Extracted 1.6 eV dd excitations. Blue lines denote the associated Gaussian fits. (h) Integrated spectral weight of the 1.6 eV dd excitation. The data of as-grown $La_3Ni_2O_{7-\delta}$/LAO thin films are taken from Ref. [35].

with the corresponding total fluorescence yield (TFY) XAS. The main and satellite peaks are indicated by red and black dashed lines, respectively. Several inelastic responses can be identified: two Raman-like excitations at approximately 70 meV and 0.4 eV, together with two localized excitations at around 1 eV and 1.6 eV that merge into a broad fluorescence. As suggested in Refs. [34,35], the 70 meV feature corresponds to a spin excitation, and the 0.4 eV as well as 1 eV features are dd excitations involving electron transitions from Ni $3d_{z^2}$ to $3d_{x^2-y^2}$ and from e_g to t_{2g} orbitals, respectively. The 1.6 eV response has been identified as dd excitations related to Ni-O_{AP} hybridization. Previous O-K edge electron energy-loss spectroscopy (EELS) [17] and XAS [65] have confirmed the presence of two hybridization channels in $La_3Ni_2O_{7-\delta}$: one between Ni $3d_{x^2-y^2}$ and in-plane O $2p_{x/y}$, and the other between Ni $3d_{z^2}$ and O_{AP} $2p_z$. The 1.6 eV dd excitation corresponds to the latter one because it resonates at the XAS satellite peak and is strongly enhanced for π polarization [34,35]. It mainly involves electronic transitions between the Ni $3d_{z^2}$ orbital near the Fermi level and the Ni $3d_{z^2}$-O_{AP} $2p_z$ charge-transfer band (CTB) located about 1.6 eV below the Fermi level [61].

Figures 2(b) and 2(c) display the incident photon energy E_i-dependent RIXS maps of the two vacuum-annealed films. The Ni-L_3 XAS signals of these samples are not measurable in either the total electron yield (TEY) or TFY detection modes. While they exhibit a similar inelastic response to the as-grown film, the 1.6 eV *dd* excitations are strongly suppressed. Figure 2(d) shows the fit to the RIXS spectrum of the as-grown $La_3Ni_2O_{7-\delta}$/LAO film at $E_i = 856.7$ eV, corresponding to the XAS satellite peak (marked by the black dashed line) that enhances the 1.6 eV *dd* excitation. The magnon and bimagnon were fitted using damped harmonic oscillator (DHO) functions [66]

$$S(q,E) = A\frac{4\gamma E E_0}{(E^2 - E_0^2)^2 + (2\gamma E)^2}, \quad (1)$$

where E_0 is the undamped energy and γ is the damping rate. The elastic peak, three dd excitations, fluorescence, and charge-transfer excitations were fitted using Gaussian functions. The extracted spectral weights of the 1.6 eV dd excitation for all three films are plotted in Figs. 2(e)–2(g), with the corresponding fits shown as blue curves. Their integrated spectral weight is summarized in Fig. 2(h). Compared with the as-grown sample, the vacuum-annealed samples #1 and #2 show significant reductions of ~50% and ~58% in spectral weight, respectively, suggesting appreciable O_{AP} defects that suppress the Ni $3d_{z^2}$-O_{AP} $2p_z$ hybridization and thereby reduce the CTB DOS. Note that epitaxial strain can also tune this hybridization by modifying the out-of-plane Ni-O_{AP}-Ni bond angle [35]. Here, for samples grown on LAO substrates and subjected to identical epitaxial strain, differences in the intensity of the 1.6 eV *dd* excitation can be attributed exclusively to the oxygen content, consistent with the evolution of oxygen content across the three samples shown in Fig. 1(d).

We now turn to the spin-excitation response to oxygen deficiency. Previous RIXS studies have suggested that the spin excitations in $La_3Ni_2O_7$ originate from a spin density wave (SDW) propagation vector at $q_{\parallel} = (0.25, 0.25)$ and disperse toward the band top near $q_{\parallel} = (0,0)$ and $(0.5,0)$ [34,35]. As shown in Fig. 3(a), high-statistics RIXS measurements with an energy resolution $\Delta E \approx 32$ meV were performed to probe the spin excitations near the band top at $q_{\parallel} = (0.06,0)$. A clear peak was observed at around 70 meV in all three samples, as indicated by the gray dashed line. Although theoretical calculations predict a non-dispersive phonon mode around 65 meV [67–69], previous polarimetric RIXS measurements have demonstrated that the phonon spectral weight is nearly negligible [34]. We therefore conclude that this peak is dominated by spin excitations rather than phonons. The inset of Fig. 3(a) summarizes the undamped spin-excitation energy E_0 and the damping rate γ, extracted from fits to the RIXS spectra using the DHO function. One can see that E_0 near the magnon band top is almost independent of the oxygen content, while γ slightly increases as the oxygen content decreases.

Figures 3(b)–3(g) present a comparison of the RIXS spectra and the corresponding fitted spin excitations for the oxygen-deficient and as-grown samples measured along the two high-symmetry directions, $[H,H]$ and $[H,0]$. For details regarding the fitting procedure, please

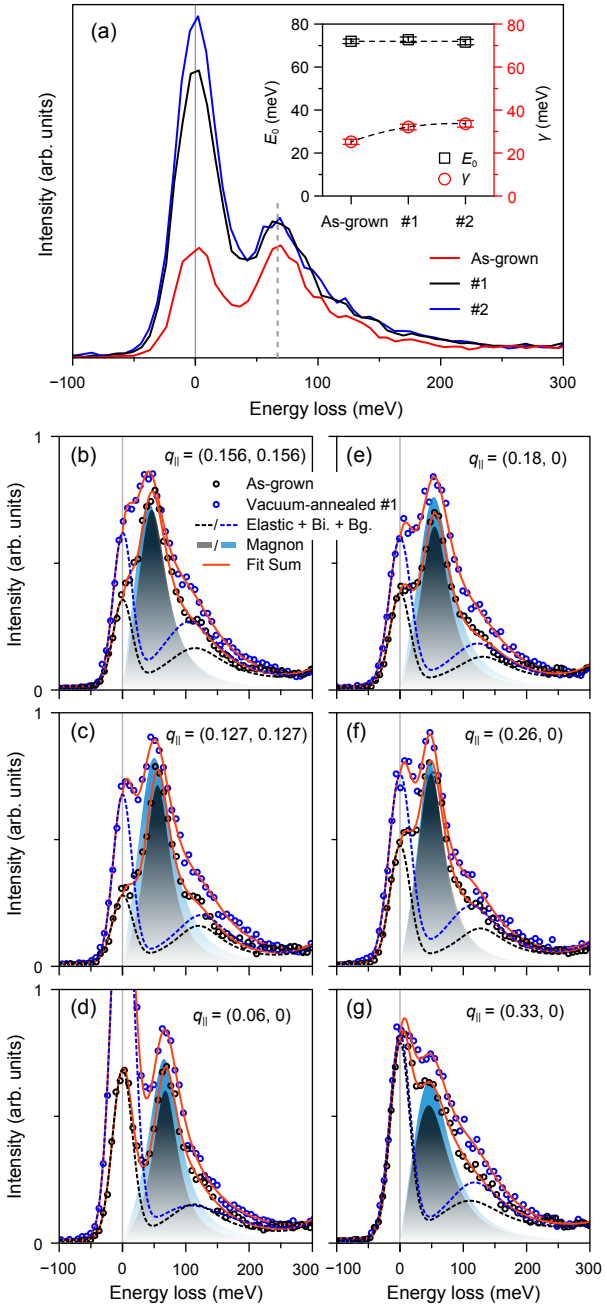

Fig. 3. (a) RIXS spectra at $q_\parallel = (0.06, 0)$ for the as-grown and vacuum-annealed $La_3Ni_2O_{7-\delta}$/LAO thin films with different oxygen concentrations. The gray dashed line indicates the peak position of the spin excitation. The inset displays the undamped magnon energy E_0 and damping rate γ fitted by a DHO function. The black dashed curves are guides to the eye. (b)–(g) Comparison of the RIXS spectra and the corresponding fits for the as-grown and vacuum-annealed $La_3Ni_2O_{7-\delta}$/LAO films measured along the $[H,H]$ and $[H,0]$ directions. The shaded areas indicate the magnon contributions. The dashed lines represent the combined contributions from the elastic line, bimagnon, and the high-energy background (tails of dd, fluorescence, and charge-transfer excitations), and the red solid lines represent the sum of all components. All spectra were normalized to the incident photon flux. The data of as-grown $La_3Ni_2O_{7-\delta}$/LAO thin films are taken from Ref. [35].

refer to the methodology described in Fig. 2(d). Here, the dashed lines represent the total contribution from the elastic peak, bimagnon, and high-energy excitations, while the shaded areas represent spin excitations. Data have been normalized to the incident photon flux. The peak positions and spectral weights of the magnons show no systematic reduction despite the presence of considerable O_{AP} defects that

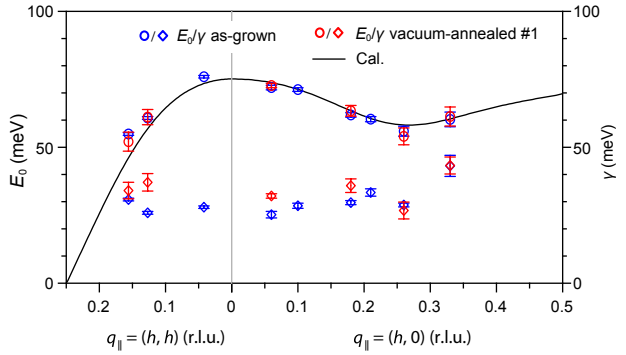

Fig. 4. Comparison of the undamped energy E_0 and the damping rate γ of the spin excitations between vacuum-annealed #1 and as-grown $La_3Ni_2O_{7-\delta}$/LAO thin films. The as-grown $La_3Ni_2O_{7-\delta}$/LAO data and the calculated magnon dispersion (black curve) are taken from Ref. [35]. Note that the vacuum-annealed (red symbols) and as-grown (blue symbols) films were measured under identical experimental conditions in the same RIXS experiment, where the scattering angles $2\theta_s$ were set to 90° and 110° to reduce the elastic scattering.

locally disrupt the interlayer superexchange pathways. These results demonstrate that such local defects do not alter the overall characteristic energy scale of the collective spin-wave excitations in $La_3Ni_2O_{7-\delta}$.

Figure 4 summarizes the undamped energy E_0 and the damping rate γ of the spin excitations for the vacuum-annealed sample #1 and the as-grown $La_3Ni_2O_{7-\delta}$/LAO thin film. Based on the classical Heisenberg model

$$H = \sum_{i<j} J_{ij} \boldsymbol{S}_i \cdot \boldsymbol{S}_j, \tag{2}$$

the black curve indicates the spin-wave dispersion calculated using the SpinW code [35,55]. Overall, the vacuum-annealed $La_3Ni_2O_{7-\delta}$/LAO film exhibits spin-excitation characteristics that are largely similar to those of the as-grown sample. On the one hand, the spin-wave dispersion of the vacuum-annealed sample closely overlaps with that of the as-grown sample and agrees well with the calculated dispersion. Although apical-oxygen vacancies locally interrupt the interlayer superexchange pathways, the collective spin-wave modes remain robust, with their characteristic energy scale nearly unaffected. On the other hand, the spin-excitation dispersion in the vacuum-annealed sample, similar to that of the as-grown film, shows a tendency to converge toward $Q = (0.25, 0.25)$, implying the persistence of SDW order with this propagation wavevector. This behavior is consistent with Monte Carlo simulations, which indicate a mixed DSS/SCS magnetic ground state within the range $0 < \delta < 0.5$ [55], where both orders are characterized by the same magnetic propagation wavevector $Q_{SDW} = (0.25, 0.25)$.

Since RIXS primarily probes short-range spin correlations, the fact that oxygen-deficient samples exhibit the same spin excitation dispersion as the as-grown sample implies that appreciable oxygen vacancies exert a negligible impact on the short-range spin correlations in $La_3Ni_2O_{7-\delta}$. Dynamical mean-field theory has revealed that vacancies promote local magnetic moments, whose random distribution further degrades electronic coherence [57]. This effect manifests as a slight increase in the damping factor [Fig. 3(a)]. Specifically, oxygen vacancies introduce both lattice disorder and a random distribution of local magnetic moments, which collectively account for the observed reduction in spin excitation lifetimes.

Studies on epitaxial strain and chemical doping have established that the interlayer superexchange J_z in nickelates is intimately coupled to the Ni $3d_{z^2}$–O_{AP} $2p_z$ hybridization. Specifically, the suppression of the 1.6 eV dd excitation—induced either by tensile strain in $La_3Ni_2O_7/SrTiO_3$ [35] or hole-overdoping in $La_{2.62}Sr_{0.38}Ni_2O_7$/SLAO [70]—consistently leads to a significant reduction in J_z and spin excitation bandwidth and spectral weight. Here, the reduced spectral weight of the 1.6 eV dd excitation in the oxygen-deficient samples [Fig. 2(h)] reflects the presence of O_{AP} vacancies. These vacancies locally disrupt the interlayer p–d hybridization and Ni-O_{AP}-Ni

superexchange pathways at their sites. Surprisingly, however, this local destruction of J_z does not reduce the energy scale or spectral weight of spin excitations. Rather, they remain nearly identical to those of the as-grown samples. This is reminiscent of doped cuprates, where the high-energy spin-excitation dispersion was also found to be independent of doping [71–74]. Nevertheless, it is noteworthy that, in contrast to cuprates, the spin-excitation dispersion in $La_3Ni_2O_{7-\delta}$ remains robust not only against electron doping but also against the local disruption of J_z. This implies that the underlying physical mechanism in nickelates is more complex than that in cuprates and goes beyond a simple picture based on doping-insensitive magnetic exchange interactions in cuprates [73].

Such robustness of spin excitations against oxygen vacancies in $La_3Ni_2O_{7-\delta}$ likely relates to the response of the magnetic ground state to oxygen vacancies. Monte Carlo simulations reveal that spinless sites introduced by oxygen vacancies drive the $La_3Ni_2O_{7-\delta}$ ground state to transition from a DSS order to a mixed DSS/SCS state within the range of $0 < \delta < 0.5$ [55]. Since the two magnetic orders share the same magnetic unit cell and propagation vector, they exhibit highly analogous spin correlations and excitation dispersions [34]. As a result, strong coupling between the two orders allows the mixed DSS/SCS ground state to preserve short-range spin correlations even when local exchange interactions J_z are disrupted by O_{AP} vacancies.

Further considering the interplay between magnetic order and superconductivity, a clear distinction emerges between bilayer nickelates and cuprate superconductors. In cuprates, antiferromagnetic (AFM) order is typically completely suppressed by doping before the superconducting dome is reached [75]. In contrast, in bilayer nickelates, although superconductivity also weakens the AFM order, the two states can still coexist over a finite range [76–78]. This behavior is reminiscent of iron-based superconductors, where AFM order coexists and competes with superconductivity in the underdoped regime [79]. Since both superconducting pairing and AFM correlations involve electronic states near the Fermi level, this competition and coexistence likely originate from a common electronic-structure feature shared by bilayer nickelates and iron-based superconductors, namely their multi-orbital character, with both relatively localized and more itinerant electronic states contributing to the Fermi surface.

In summary, we have investigated the electronic and spin excitations in $La_3Ni_2O_{7-\delta}$ thin films using Ni-L_3 edge RIXS. In the oxygen-deficient samples, O_{AP} vacancies disrupt the local interlayer p–d hybridization and the interlayer Ni-O_{AP}-Ni superexchange pathway. Despite the dilution of J_z, the spin excitation dispersion and spectral weight remain essentially unaffected, in contrast to the results observed in $La_3Ni_2O_{7-\delta}/SrTiO_3$ [35] and $La_{2.62}Sr_{0.38}Ni_2O_7$/SLAO [70], where the suppression of Ni–O p–d hybridization leads to a pronounced softening of the spin-excitation dispersion and a strong reduction of its spectral weight. These results suggest that short-range spin correlations in $La_3Ni_2O_{7-\delta}$ are insensitive to oxygen-vacancy-induced perturbations, including electron doping and local disruption of interlayer superexchange pathways, within the mixed DSS/SCS ground state. As spin excitations have been found to be closely linked to superconductivity in bilayer nickelates [35,70], these findings rule out the possibility that appreciable oxygen defects suppress superconductivity only by inhibiting interlayer antiferromagnetic superexchange interactions and spin fluctuations, and highlight that an appropriate electronic structure and possibly electronic coherence may also be critical.

Acknowledgements

This work was supported by the Scientific Research Innovation Capability Support Project for Young Faculty (Grant No. ZYGXQNJSKYCXNLZCXM-M2), the National Natural Science Foundation of China (Grant Nos. 12574142, 12434002, and 125B2073), the National Key Projects for Research and Development of China (Grant No. 2021YFA1400400), and the Natural Science Foundation of Jiangsu Province (Grant No. BK20233001). The work at PSI is supported by the Swiss National Science Foundation (Grant No. 207904). We acknowledge the European Synchrotron Radiation Facility (ESRF) for providing synchrotron radiation facilities (Proposal No. SC-5699) at the ID32 beamline.

References

[1] Sun H, Huo M, Hu X, Li J, Liu Z, Han Y, Tang L, Mao Z, Yang P, Wang B, Cheng J, Yao D X, Zhang G M, and Wang M 2023 *Nature* **621** 493
[2] Taniguchi S, Nishikawa T, Yasui Y, Kobayashi Y, Takeda J, Shamoto S-I, and Sato M 1995 *J. Phys. Soc. Jpn.* **64** 1644
[3] Zhang Z, Greenblatt M, and Goodenough J B 1994 *J. Solid State Chem.* **108** 402
[4] Gao R, Jin L, Huyan S, Ni D, Wang H, Xu X, Budko S L, Canfield P, Xie W, and Cava R J 2024 *ACS Appl. Mater. Interfaces* **16** 66857
[5] Poltavets V V, Lokshin K A, Egami T, and Greenblatt M 2006 *Mater. Res. Bull.* **41** 955
[6] Zhou Y, Guo J, Cai S, Sun H, Li C, Zhao J, Wang P, Han J, Chen X, Chen Y, Wu Q, Ding Y, Xiang T, Mao H K, and Sun L 2025 *Matter Radiat. Extremes* **10** 027801
[7] Ueki Y, Sakurai H, Nagata H, Yamane K, Matsumoto R, Terashima K, Hirose K, Ohta H, Kato M, and Takano Y 2025 *J. Phys. Soc. Jpn.* **94** 013703
[8] Zhang Y, Su D, Huang Y, Shan Z, Sun H, Huo M, Ye K, Zhang J, Yang Z, Xu Y, Su Y, Li R, Smidman M, Wang M, Jiao L, and Yuan H 2024 *Nat. Phys.* **20** 1269
[9] Dong Z, Wang G, Wang N, Dong W H, Gu L, Xu Y, Cheng J, Chen Z, and Wang Y 2025 *Nat. Mater.* **24** 1927
[10] Wang G, Wang N N, Shen X L, Hou J, Ma L, Shi L F, Ren Z A, Gu Y D, Ma H M, Yang P T, Liu Z Y, Guo H Z, Sun J P, Zhang G M, Calder S, Yan J Q, Wang B S, Uwatoko Y, and Cheng J G 2024 *Phys. Rev. X* **14** 011040
[11] Li F, Xing Z, Peng D, Dou J, Guo N, Ma L, Zhang Y, Wang L, Luo J, Yang J, Zhang J, Chang T, Chen Y S, Cai W, Cheng J, Wang Y, Liu Y, Luo T, Hirao N, Matsuoka T, Kadobayashi H, Zeng Z, Zheng Q, Zhou R, Zeng Q, Tao X, and Zhang J 2026 *Nature* **649** 871
[12] Ko E K, Yu Y, Liu Y, Bhatt L, Li J, Thampy V, Kuo C T, Wang B Y, Lee Y, Lee K, Lee J S, Goodge B H, Muller D A, and Hwang H Y 2025 *Nature* **638** 935
[13] Zhou G, Lv W, Wang H, Nie Z, Chen Y, Li Y, Huang H, Chen W, Sun Y, Xue Q K, and Chen Z 2025 *Nature* **640** 641
[14] Hao B, Wang M, Sun W, Yang Y, Mao Z, Yan S, Sun H, Zhang H, Han L, Gu Z, Zhou J, Ji D, and Nie Y 2025 *Nat. Mater.* **24** 1756
[15] Liu Y, Ko E K, Tarn Y, Bhatt L, Li J, Thampy V, Goodge B H, Muller D A, Raghu S, Yu Y, and Hwang H Y 2025 *Nat. Mater.* **24** 1221
[16] Zhou G, Wang H, Huang H, Chen Y, Peng F, Lv W, Nie Z, Wang W, Jia J F, Xue Q K, and Chen Z 2026 *Natl. Sci.Rev.* **13** nwag151
[17] Dong Z, Huo M, Li J, Li J, Li P, Sun H, Gu L, Lu Y, Wang M, Wang Y, and Chen Z 2024 *Nature* **630** 847
[18] Liu Z, Huo M, Li J, Li Q, Liu Y, Dai Y, Zhou X, Hao J, Lu Y, Wang M, and Wen H H 2024 *Nat. Commun.* **15** 7570
[19] Yang J, Sun H, Hu X *et al*. 2024 *Nat. Commun.* **15** 4373
[20] Luo Z, Hu X, Wang M, Wú W, and Yao D X 2023 *Phys. Rev. Lett.* **131** 126001
[21] Zhang Y, Lin L F, Moreo A, and Dagotto E 2023 *Phys. Rev. B* **108** L180510
[22] Christiansson V, Petocchi F, and Werner P 2023 *Phys. Rev. Lett.* **131** 206501
[23] Lechermann F, Gondolf J, Bötzel S, and Eremin I M 2023 *Phys. Rev. B* **108** L201121
[24] Shilenko D A and Leonov I V 2023 *Phys. Rev. B* **108** 125105
[25] Cao Y and Yang Y f 2024 *Phys. Rev. B* **109** L081105
[26] Lechermann F, Bötzel S, and Eremin I M 2024 *Phys. Rev. Mater.* **8** 074802
[27] Li J, Peng D, Ma P, Zhang H, Xing Z, Huang X, Huang C, Huo M, Hu D, Dong Z, Chen X, Xie T, Dong H, Sun H, Zeng Q, Mao H K, and Wang M 2025 *Natl. Sci. Rev.* **12** nwaf220
[28] Bednorz J G and Müller K A 1986 *Z. Phys. B* **64** 189
[29] Anderson P W 1987 *Science* **235** 1196
[30] Lee P A, Nagaosa N, and Wen X G 2006 *Rev. Mod. Phys.* **78** 17
[31] Keimer B, Kivelson S A, Norman M R, Uchida S, and Zaanen J 2015

Nature **518** 179
[32] Sakakibara H, Suzuki K, Usui H, Miyao S, Maruyama I, Kusakabe K, Arita R, Aoki H, and Kuroki K 2014 *Phys. Rev. B* **89** 224505
[33] Li W M, Zhao J, Cao L P *et al*. 2019 *Proc. Natl. Acad. Sci. U.S.A.* **116** 12156
[34] Chen X, Choi J, Jiang Z, Mei J, Jiang K, Li J, Agrestini S, Garcia-Fernandez M, Sun H, Huang X, Shen D, Wang M, Hu J, Lu Y, Zhou K J, and Feng D 2024 *Nat. Commun.* **15** 9597
[35] Zhong H, Hao B, Zhang Z *et al*. 2025 arXiv:2502.03178 [cond-mat.supr-con]
[36] Lu C, Pan Z, Yang F, and Wu C 2024 *Phys. Rev. Lett.* **132** 146002
[37] Qu X Z, Qu D W, Chen J, Wu C, Yang F, Li W, and Su G 2024 *Phys. Rev. Lett.* **132** 036502
[38] Oh H and Zhang Y H 2023 *Phys. Rev. B* **108** 174511
[39] Tian Y H, Chen Y, Wang J M, He R Q, and Lu Z Y 2024 *Phys. Rev. B* **109** 165154
[40] Chen J, Yang F, and Li W 2024 *Phys. Rev. B* **110** L041111
[41] Ouyang Z, Wang J M, Wang J X, He R Q, Huang L, and Lu Z Y 2024 *Phys. Rev. B* **109** 115114
[42] Lu C, Zhang M, Pan Z, Wu C, and Yang F 2025 *Commun. Phys.* **8** 354
[43] Qu X Z, Qu D W, Yi X W, Li W, and Su G 2025 *Phys. Rev. B* **112** L161101
[44] Sakakibara H, Kitamine N, Ochi M, and Kuroki K 2024 *Phys. Rev. Lett.* **132** 106002
[45] Shen Y, Qin M, and Zhang G M 2023 *Chin. Phys. Lett.* **40** 127401
[46] Yang Y F, Zhang G M, and Zhang F C 2023 *Phys. Rev. B* **108** L201108
[47] Qin Q and Yang Y F 2023 *Phys. Rev. B* **108** L140504
[48] Luo Z, Lv B, Wang M, Wú W, and Yao D X 2024 *npj Quantum Mater.* **9** 61
[49] Kaneko T, Sakakibara H, Ochi M, and Kuroki K 2024 *Phys. Rev. B* **109** 045154
[50] Zheng Y Y and Wú W 2025 *Phys. Rev. B* **111** 035108
[51] Kakoi M, Kaneko T, Sakakibara H, Ochi M, and Kuroki K 2024 *Phys. Rev. B* **109** L201124
[52] Shen Y, Huang J, Qian X, Zhang G M, and Qin M 2025 *Phys. Rev. B* **111** L180508
[53] Wang J and Yang Y F 2025 *Phys. Rev. B* **111** 014512
[54] Wang M, Hao B, Sun W, Yan S, Sun S, Zhang H, Gu Z, and Nie Y 2026 *Phys. Rev. Lett.* **136** 066002
[55] Ni X S, Ji Y, He L, Xie T, Yao D X, Wang M, and Cao K 2025 *npj Quantum Mater.* **10** 17
[56] Liu Y B, Mei J W, Ye F, Chen W Q, and Yang F 2023 *Phys. Rev. Lett.* **131** 236002
[57] Jiang P, Li J, Cao Y H *et al*. 2025 arXiv:2512.00301 [cond-mat.supr-con]
[58] Wang Y, Chen Z, Zhang Y *et al*. 2025 arXiv:2501.08536 [cond-mat.str-el]
[59] Tarn Y, Liu Y, Theuss F, Li J, Wang B Y, Bhatt L, Wang J, Song J, Thampy V, Goodge B H, Muller D A, Shen Z X, Yu Y, and Hwang H Y 2026 *Adv. Mater.* **38** e20724
[60] Ament L J P, van Veenendaal M, Devereaux T P, Hill J P, and van den Brink J 2011 *Rev. Mod. Phys.* **83** 705
[61] Wú W, Luo Z, Yao D X, and Wang M 2024 *Sci. China Phys. Mech. Astron.* **67** 117402
[62] Osada M, Terakura C, Kikkawa A, Nakajima M, Chen H Y, Nomura Y, Tokura Y, and Tsukazaki A 2025 *Commun. Phys.* **8** 251
[63] Nie Z, Li Y, Lv W, Xu L, Jiang Z, Fu P, Zhou G, Song W, Chen Y, Wang H, Huang H, Lin J, Jia J F, Shen D, Li P, Xue Q K, and Chen Z 2026 *Nature* **652** 628
[64] Puphal P, Reiss P, Enderlein N, Wu Y M, Khaliullin G, Sundaramurthy V, Priessnitz T, Knauft M, Suthar A, Richter L, Isobe M, van Aken P A, Takagi H, Keimer B, Suyolcu Y E, Wehinger B, Hansmann P, and Hepting M 2024 *Phys. Rev. Lett.* **133** 146002
[65] Ren X, Sutarto R, Wu X, Zhang J, Huang H, Xiang T, Hu J, Comin R, Zhou X, and Zhu Z 2025 *Commun. Phys.* **8** 52
[66] Lu X, Zhang W, Tseng Y, Liu R, Tao Z, Paris E, Liu P, Chen T, Strocov V N, Song Y, Yu R, Si Q, Dai P, and Schmitt T 2022 *Nat. Phys.* **18** 806
[67] Ouyang Z, Gao M, and Lu Z Y 2024 *npj Quantum Mater.* **9** 80
[68] Zhan J, Gu Y, Wu X, and Hu J 2025 *Phys. Rev. Lett.* **134** 136002
[69] You J Y, Zhu Z, Del Ben M, Chen W, and Li Z 2025 *npj Comput. Mater.* **11** 3
[70] Zhong H, Hao B, Chen A, Huang X, Li C, Zhang W, Liu C, Kummer K, Brookes N, Nie Y, Schmitt T, and Lu X 2026 arXiv:2603.01120 [cond-mat.supr-con]
[71] Dean M P M, Dellea G, Springell R S, Yakhou-Harris F, Kummer K, Brookes N B, Liu X, Sun Y J, Strle J, Schmitt T, Braicovich L, Ghiringhelli G, Bozovic I, and Hill J P 2013 *Nat. Mater.* **12** 1019
[72] Le Tacon M, Minola M, Peets D C, Moretti Sala M, Blanco-Canosa S, Hinkov V, Liang R, Bonn D A, Hardy W N, Lin C T, Schmitt T, Braicovich L, Ghiringhelli G, and Keimer B 2013 *Phys. Rev. B* **88** 020501
[73] Le Tacon M, Ghiringhelli G, Chaloupka J, Moretti Sala M, Hinkov V, Haverkort M W, Minola M, Bakr M, Zhou K J, Blanco-Canosa S, Monney C, Song Y T, Sun G L, Lin C T, De Luca G M, Salluzzo M, Khaliullin G, Schmitt T, Braicovich L, and Keimer B 2011 *Nat. Phys.* **7** 725
[74] Li X T, Tu S J, Chaix L, Fawaz C, d'Astuto M, Li X, Yakhou-Harris F, Kummer K, Brookes N B, Garcia-Fernandez M, Zhou K J, Lin Z F, Yuan J, Jin K, Dean M P M, and Liu X 2024 *Phys. Rev. Lett.* **132** 056002
[75] Lee P A, Nagaosa N, and Wen X G 2006 *Rev. Mod. Phys.* **78** 17
[76] Zhang S, Zhang M, Luo Q *et al*. 2026 arXiv:2604.14701 [cond-mat.supr-con]
[77] Chen X, Zhang W, Peng F *et al*. 2026 arXiv:2604.21899 [cond-mat.supr-con]
[78] Meng Y, Yang Y, Sun H, Zhang S, Luo J, Chen L, Ma X, Wang M, Hong F, Wang X, and Yu X 2024 *Nat. Commun.* **15** 10408
[79] Dai P 2015 *Rev. Mod. Phys.* **87** 855